COUPLED SHIP AIRWAKE AND ROTOR AIRLOADS SIMULATION METHODOLOGY

Gregorio Frassoldati, Leonardo Helicopters, Cascina Costa (VA), Italy *(/ Università degli Studi Roma Tre)*
Cristiano Capizzi, Leonardo Helicopters, Cascina Costa (VA), Italy
Prederi Davide, Leonardo Helicopters, Cascina Costa (VA), Italy
Stefano Melone, Leonardo Helicopters, Cascina Costa (VA), Italy

Abstract

This paper gathers the experience gained in exploring the possible setups for a new computational methodology to evaluate the aerodynamic field on ship decks. With respect to the legacy approach used in Leonardo Helicopters Division, the new workflow tries to erode the conservativism limits assumed on the results by improving the accuracy of the outcomes. All steps of have been tailored to be as general as possible, in order to be automatable for industrial applications. The main impact of the improvement in aerodynamics will be presented through its effect on the rotor loads during start-up manoeuvers.

1. NOTATION

Hereafter the most used symbols and acronyms can be found listed in alphabetical order.

Symbols:

k	Turbulence kinetic energy [J/kg]
ε	Rate of dissipation [J/kg·s]
ω	Specific rate of dissipation [1/s]
u	Velocity [m/s]
Δt	Timestep [s]
Δx	Differential distance [m]
Ls	Ship overall Length [ft]

Acronyms:

AW	AgustaWestland
BC	Boundary Condition
CFD	Computational Fluid Dynamics
CFL	Courant-Friedrichs-Lewy
DDES	Delayed Detached Eddy Simulation
DES	Detached Eddy Simulation
ISA	International Standard Atmosphere
LES	Large Eddy Simulation
LHD	Leonardo Helicopters Division
RANS	Reynolds-Averaged Navier-Stokes
SAS	Scale-Adaptive Simulation
SBES	Stress-Blended Eddy Simulation
SDR	Specific Dissipation Rate
SL	Sea Level
SRS	Scale Resolving Simulation
TBL	Turbulent Boundary Layer
TKE	Turbulent Kinetic Energy
TVR	Turbulent Viscosity Ratio
URANS	Unsteady RANS

2. INTRODUCTION

Ship operations represents for rotary-wing aircrafts one of the most demanding scenarios from an operational point of view. Moving towards certification by simulation and digital twins covering the whole aircraft life cycle, being able to properly capture even such complex scenarios becomes a concrete objective. This study represents an important step in that direction, aiming to describe a computational methodology to evaluate the aerodynamic field on ship decks and its impact on rotor loads applications during start-up manoeuvers. The drive for accuracy naturally comes from the desired output estimation, but it must be borne in mind that each point taken away from accuracy goes in favor to computational time. Technical analyses are always subject to the pace given to the whole program: from there comes the need for an efficiency/accuracy tradeoff study.

From an aerodynamic standpoint, the bluff-body separations taking place downstream of most elements on deck, along with separating shear layers and vortices interactions, makes the problem the most specific and case-dependent for a helicopter operational environment. The first step of this study is an investigation into several numerical setups, presenting limits and advantages of the possible modeling of the airwake. Once a promising setup had been found, simulations for unsteady data acquisitions at different azimuthal directions of the incoming wind were performed, and their results compared with respect to a legacy approach. These data have then been tested and compared in generating wind boxes for aeroelastic simulations for rotor start-ups, giving the sense of the actual impact of such formulations on rotorcraft applications.

3. PROBLEM DESCRIPTION

3.1. Aerodynamics Perspective

Several studies, among which [1] and [2], tried to assess the problem correlating wind tunnel experimental campaigns with computational fluid dynamics simulations, providing resourceful insights and databases for literature ship models, such as the SFS and the SFS2 (as thoroughly explained in [1], Simple Frigate Shape, first and second model respectively). From that reference geometry, this investigation has the objective to find general guidelines to approach the study of an arbitrarily shaped ship.

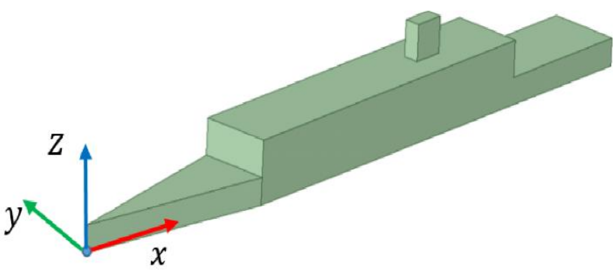

Figure 1: SFS2 model

Naval ship operations are often demanding for helicopters as clearly demonstrated in [3] and [4], and the effects they have on helicopters design influence different aspects of their operational life. From landing manoeuvres, described in [5], to rotor startup procedures, the impact of the turbulent airwake acting on the deck is highly influencing; from there comes the need to know the frequency content, the topological aspect of the wake and the interactions with the aircraft aerodynamics. For this reason, the possible CFD setups in literature explored different possibilities for SRS to assess the preservation of the energy content for diverse frequencies, as in [6], [7] and [8]. The present study took into account all past explorations of the spectrum of possibilities.

Flight handling qualities, as well as airloads, are strongly affected by this unsteady flow field, whose peculiarity changes from one ship to another as well as with the relative angle between the ship orientation and the incoming wind.

Naturally, the specificity of the output expected from every single specific analysis is the only determinant factor in the quality requests. It is also true, however, that the airwake retains the same characteristics regardless of the output: therefore a few salient aspects are key factors is justifying the need for this study. Moreover, the real added value is the optimisation of the process, made possible by the comprehension of the physics of the problem at hand and the consequences of each single choice in the steps followed during the building process of the analysis to perform.

3.2. Rotor Loads Perspective

Subsequently, this study will attempt to find the best possible strategy to study the impact of said airwakes on airloads estimation of the rotors of helicopters stationing on deck. Many literature references approached the wide world of ship operations; in [9] the airloads on the rotor are the object of the study, and in [10] the effect of unsteady wakes on loads considers both rotors and fuselage, and its effect on pilot workload during flight close to ships. The peculiar application presented here, however, will be compared with respect to the legacy approach internal to the company for the specific application of start-up procedures.

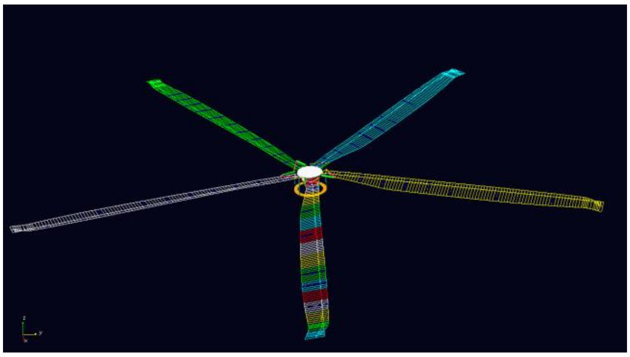

Figure 2: main rotor aeroelastic model used for start-up manoeuvers analyses

The airloads acting on the rotors become particularly relevant in the startup procedure because rotor blades do not benefit of the centrifugal stiffening contribution and therefore are more prone to flapping motions and flap/droop stop contacts. Along with that, the absence of inertial stiffness makes also the blades sensible to dangerous resonance fenomena, and the frequency content of the airwake can become relevant for those evaluations.

4. AERODYNAMICS METHODOLOGY ESTABLISHMENT PROCESS

4.1. General

The aerodynamic analyses have been carried out by means of finite volumes CFD simulations, exploring diverse possibilities in terms of meshing, numerical schemes, timestep and computational performance. The results have been referenced to the intended function of the data produced, in terms of the effect of the airspeed fluctuations on airloads estimation.

4.2. Computational Domain

The literature available proposed a variety of possible scenarios for the domain description, and here is where the need to optimise the methodology was most felt since the beginning. From [1] and [6] appeared as evident the need to have a domain where the boundary conditions were imposed at about five times the main dimension of the ship model, given that it seemed the least dimension sizing were the field gradients of the BC imposition were not affecting anymore the flow topology and development. Some studies, such as [7], proposed a different approach based on a scaled model, interesting for the SFS2 specific case, which is not completely Reynolds-driven in its methodology (as clarified in [11]), but the limitation in the applicability on other geometries and test cases made it less relevant to the purpose of this study. This fact comes from a fundamental need in this kind of simulations: the airloads need to be mapped for all possible azimuths of incoming wind, which makes this problem even more comprehensive in terms of computational domain.

In fact, in the industrial approach to ship operations for helicopters on deck, the investigation must pursue different wind velocities and all possible azimuths, because otherwise either the helicopters utility or the ship usage clearance would have to be limited. This makes the number of simulations required for each aircraft-ship combination to rise conspicuously. Literature is rich of examples of CFD derived data for piloted simulations; one of the first studies is paper [12], which led to many other instances of building and validating an entirely simulative environment, whose purposes can actually vary.

How to build the best possible mesh was nonetheless an interesting task to fulfill: the impact on the computational time in a real-life application was not negligible at all. Since the ultimate objective was to assess a methodology widely applicable, the natural choice for volumetric elements was a fully unstructured mesh. Real life applications of CFD study of ships need to take into account a plethora of possible structures, with various sizes and shapes, and therefore building a structured mesh of sufficient qualities inside the usual time schedule requested in companies is often unfeasible. For the very same reason the choice of triangular surface elements was the simplest one to allow the simulation of arbitrary shaped elements.

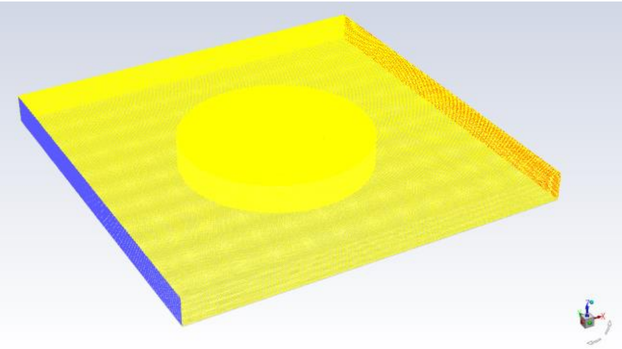

Figure 3: whole domain zones discretization

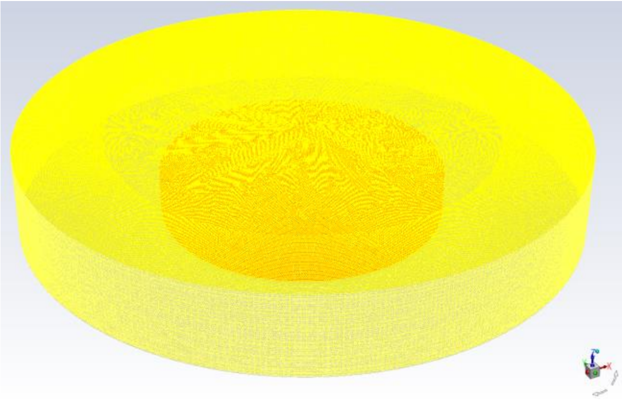

Figure 4: cylinder zones discretization

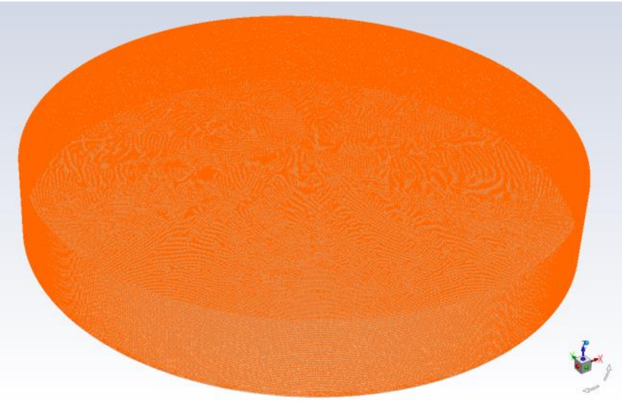

Figure 5: inner cylinder zone outer mesh

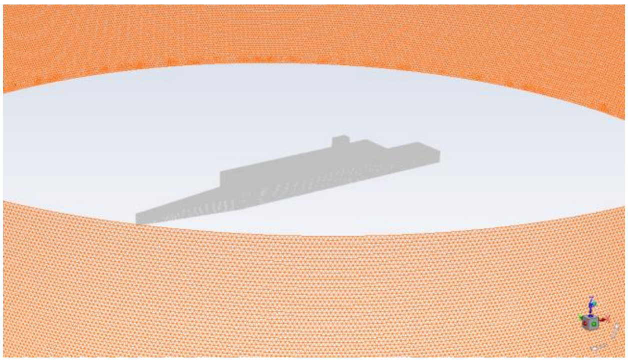

Figure 6: ship mesh positioning inside the domain

Let us outline the implemented steps to research the best possible industrial workflow to assess the problem. The basic requirements were these:

- The domain description needed to be as general as possible. The same domain needed to be built just once, to be able to adapt to all possible incoming azimuths of the wind, to have the possibility to comprehend different scenarios and modeling needs.
- The mesh building process needed to be applicable to all possible ship geometries from scratch, depending on the problem at hand and on the client of the analysis. The model needed to be efficient also in terms of cell generation, modeling those features that do not affect excessively the quality of the solution. Moreover, the most parts of the domain common between different cases, the better.

This two points were utterly relevant to limit the computational cost of such analyses, given the direct link existing between mesh size and memory request, influencing then the computational time. Along with that, the generality of the domain potentially saves hours in preprocessing and case-building. Therefore, the best outcome was made of a domain of this kind:

- an outer box with side long 5Ls (Ls = length of the ship, in this case 455 [ft]) boxed with a cutcell approach, as to exploit the regularity of such geometry and saving cells in the least relevant area. This box is 0.75Ls tall and holed in the center.
- an inner cylinder of diameter 2.5Ls meshed with hexahedral approach, once again to save cells, helped from a tetrahedral buffer layer in order to be able to adapt to its boundaries and peel layers for a smooth size change transition. This cylinder is 0.75Ls tall as well, but has a cut out portion in the lower central region.
- a smaller cylinder inside the first one, 0.375Ls tall and with 1.25Ls diameter, meshed in smaller hexahedral elements enclosing the ship itself and its volumetric prism layers (which topologically constitute the inner volume region).

The outer box helped the simplification of BCs, having always the same inlet and the same outlet; therefore, the same BCs can be kept for all azimuths simulated at the same airspeed. Moreover, splitting the outer mesh, apart from helping in saving cell count with different refinements, allows the analyst to avoid generating different cases of changing anything among different conditions.

In particular, given the possibility to establish non-conformal interfaces in *Ansys Fluent* ©, the azimuth angle can be imposed simply by rotating the outer box with respect to the inner mesh; being extremely light in cell count, the operation is extremely agile and fast to perform. Such shrewdness can become relevant in saving computational times for industrial applications, when there is the need to perform hundreds of CFD cases for each ship geometry.

The mesh refinement was guided by the needs of the results. The subdivision of the cylinder into an outer and an inner cylinder helped one more time to save cells and preprocessing time; in particular, down to the inner cylinder, which actually comprehends the ship geometry, all the other volume zones can be saved and then reused for all ships of the same class and similar length. This is yet another advantage of such approach.

A practical example would be the simulation of an aircraft carrier ship, where the long deck could make prism layers and wall turbulence management relevant. In such a case, the entire domain apart from the inner cylinder could be built just once, and only the zone enclosing the ship's geometry be adjusted depending on the freestream wind velocity (given the different requirements for wall management).

Furthermore, the subdivision in inner and outer cylinder intrinsically works as a direction-insensitive refinement region, making the mesh once more suited for all-azimuth simulations.

As general rule, per legacy approach, in aerodynamic load estimation the flow field needs to be discretised at over 20 locations per blade radius. For establishing the best CFD setup, a fictional main rotor centered at 5 [m] from the ground and with a 6 [m] main rotor radius was chosen; this would correspond to a 30 [cm] discretised volume region. (It is important to notice that the example rotor used for the methodology optimisation is not the same used in the aeroelastic study, where an actual main rotor architecture from AW lines was used to evaluate the outcomes in a more relevant manner). From there, a refinement box was imposed inside the inner cylinder, right above the deck where the helicopter is supposed to be on the ship, and as general as possible with respect to incoming wind.

Such refined region is intended to include all possible motions of the blade during the subsequent aeroelastic analysis, and on the cell zones node the values of x velocity, y velocity and z velocity will be collected to build the wind maps used for the aforementioned coupled simulation.

After an initial study via RANS simulations on different introductory meshes, it became clear that all superstructures on the ship deck needed to be included in a ship refinement region, in order to avoid excessive TVR in the separated zone; that also helped preserving the correct wake structure down to the helicopters location without excessive dissipation. Specifically, a refinement box of sizes Ls *x* Ls/4 *x* Ls/4 was defined and centered at (Ls/4, 0, Ls/8), being *z=0* the sea surface.

Then, following all these indications and findings listed above, two different meshes, being the best candidates, were chosen to be tested with different numerics in order to find the best overall compromise between accuracy and efficiency.

In conclusion, the result would look like this:

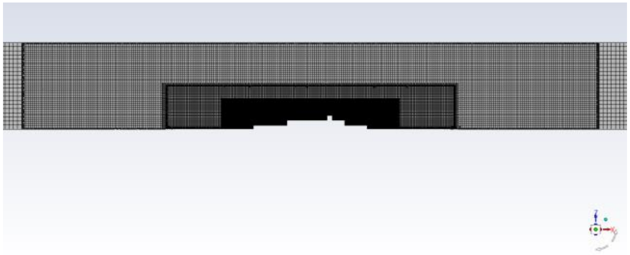

Figure 7: high resolution mesh (y=0 plane)

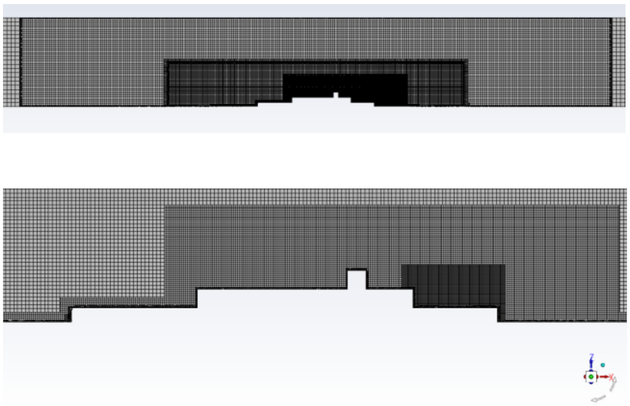

Figure 8 a) and b): low resolution mesh (y=0 plane)

The outer box is the only one with quadrangular faces all around its surfaces and its sides are discretized into 140 cubic cells. With the inner cylindrical hole, the total count of cells for the outer box is 2M elements.

The high resolution mesh encloses the entire ship geometry with the same mesh resolution required for the rotor zone. This led to a mesh cell count of around ~71M, against the ~13M cells of the low resolution mesh.

4.3. Numerical Setup

In terms of boundary conditions imposed on the surface zones, most of the simulations exploited a no-slip wall boundary condition only on the ship surfaces, a slip wall BC on lower and upper surfaces and a pressure inlet / pressure outlet BC setup for the two faces respectively at minimum x-axis and maximum x-axis coordinate of the outer box. (Some introductory studies with different BCs to further enhance the physical representation are reported in the future works subsection). To compare properly with available literature results for the SFS2, ISA SL were considered for atmospheric conditions, with a freestream velocity of 40 [kts]. Three different azimuths were simulated: headwind, Green 45° and Green 90° wind directions. These setups were common between all simulations, while the investigation went on changing all numerical schemes about governing equations and space-time discretization.

Naturally, the first step was performing a precursor RANS simulation in order to establish a baseline with respect to legacy approach and also to evaluate the mesh quality for further steps into unsteady modeling. Through all simulation setups, the RANS turbulence closure was always operated via kw-sst model, both in RANS/URANS as well as for the unresolved portion of the domain during LES-type simulations.

The following steps sum up the procedure followed to evaluate the relationship between mesh resolution and simulation accuracy before embarking in costly transient simulations.

For a LES-type simulation is important to assess beforehand the amount of TKE that will be properly solved and not modeled via RANS turbulence closure.

The main quantity of relevance is the ratio of grid length scale to integral length scale:

$$R_L = \frac{\Delta_{max}}{L_t^{RANS}}$$

$$L_t^{RANS} = \left(\frac{k^{3/2}}{\varepsilon}\right)$$

The higher R_L, the lower resolution is provided to the simulation. (It can be clearly seen from the second formula that a two-equation turbulence method is required to evaluate the grid length scale).

Considering *L* as the smallest resolved eddy scale, and that we need at least a couple cells in each direction to solve it, the main dimension of the cells capturing such a vortex will be $\Delta = L/2$.

Table 1: Cumulative TKE vs length scale of eddies

	$\boldsymbol{L/L_0}$	L_0/Δ
k(L) = 0.1k (10%)	6.10	0.33
k(L) = 0.5k (50%)	1.60	1.25
k(L) = 0.8k (80%)	0.42	4.80
k(L) = 0.9k (90%)	0.16	12.5

The goal was to resolve 80% of the turbulent kinetic energy (that is usually the reference value for LES-like formulations); then, we need to resolve the eddies whose sizes are larger than roughly half the size of the integral length scale L_0.

It is a good practice to have at least 5 cells (rounding up 4.8) across L_0 to resolve 80% of the k spectrum; 10-12 cells per L_0 can warrant a better 90% resolution of the energy spectrum in the regions of interest.

Once defined the integral length scale, the number of cells per L_0 can be assessed assuming that

$$\Delta = \sqrt[3]{\boldsymbol{Cell_{VOLUME}}}$$

This naturally holds exactly true only for cubical cells, and becomes less and less accurate with increasing aspect ratios or with changing cell shape. For our domain, where most is covered via hexahedral elements, this is an acceptable assumption.

For the methodology optimisation study, the simulation has been run for 1000 iterations, with an equivalent CFL number of 200 (“equivalent” because in steady simulations, the CFL parameter can be considered more of an under-relaxation tuning factor); all solvers were set to second-order accuracy in space.

Table 2: Numerics Comparison

Method	Mesh	Solver	Time	Pressure	Momentum
RANS	Low Res.	Coupled	-	2nd order	2nd order
RANS	High Res.	Coupled	-	2nd order	2nd order
URANS	Low Res.	Coupled	Bounded 2nd implicit	2nd order	2nd order
SAS	Low Res.	Coupled	Bounded 2nd implicit	2nd order	Centr. Diff.
SAS	High Res.	Coupled	Bounded 2nd implicit	2nd order	Centr. Diff
SBES	Low Res.	Simplec	Bounded 2nd implicit	2nd order	Bound. C. D.
SBES	High Res.	Simplec	Bounded 2nd implicit	2nd order	Bound. C. D.

In Figure 9 and Figure 10, it can be seen that the region of interest is well resolved following this criteria, being cut out of the contoured region of the *y=0* plane.

Clipping the contour plot of the L0 over Δ ratio, the coloured zones are the ones where the TKE is under-resolved with respect to the desired target. It is worth noticing that the zone of interest (above the aft deck) was always resolved even for the low resolution mesh, also for non-headwind conditions (Figure 11 and Figure 12).

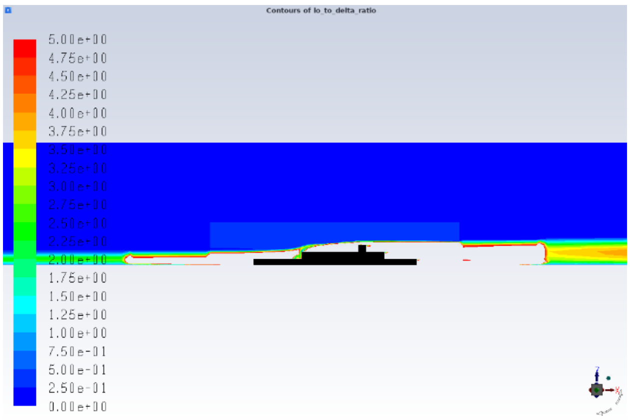

Figure 9: lengths ratio contours headwind high resolution mesh

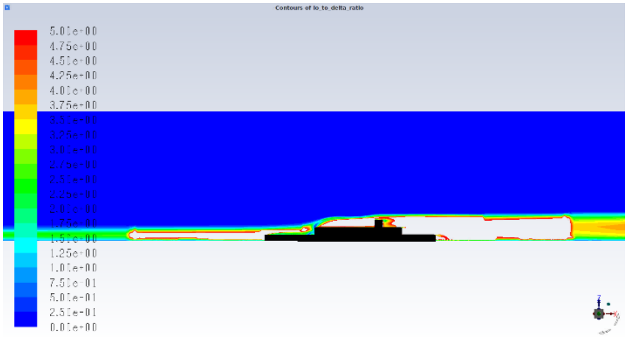

Figure 10: lengths ratio contours headwind low resolution mesh

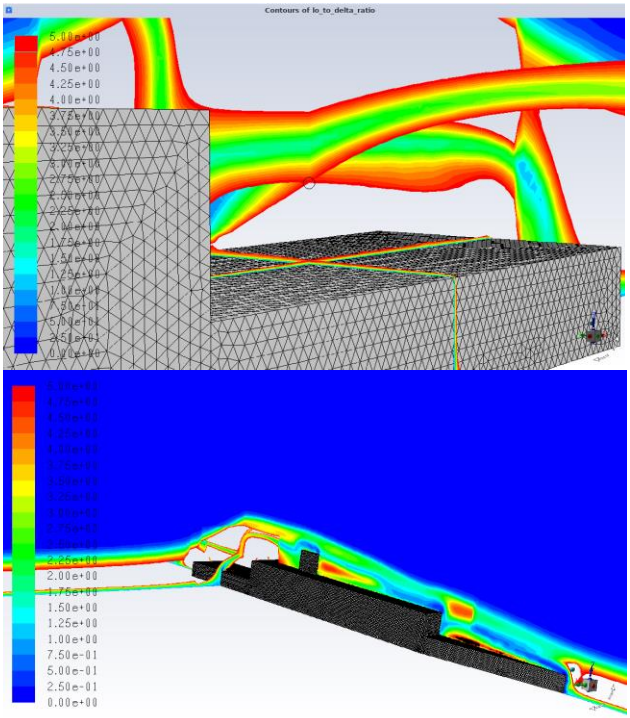

Figure 11 (a, b): lengths ratio contours for green 45 condition low resolution mesh

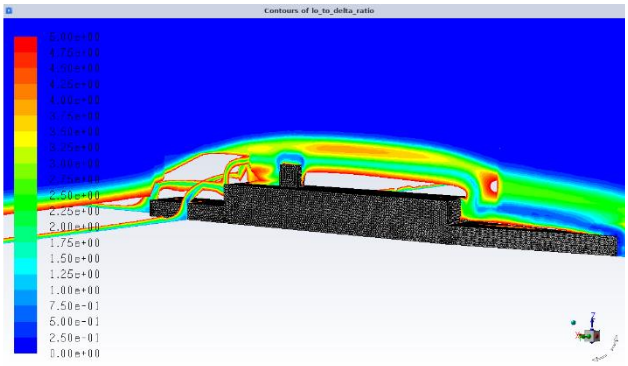

Figure 12: lengths ratio contours for green 90 condition low resolution mesh

The methodology study proceeded without any prejudice, taking into account RANS and URANS simulations as well as hybrid methods. Hybrid methods are usually well suited for globally unstable flows such as these, and giving the extreme dependency of the flow behavior on azimuth and ship geometry, standardizing guidelines for a zonal LES would have hardly been feasible.

For this reason, as far as SRS were concerned, the best-suited models were deemed to be SAS and SBES. Both models are available in (and had been developed by) Ansys Fluent ©. SBES in particular promised a fast transition to LES mode after separation, particularly relevant if the helicopter rotor extends in a zone close to where the separation happens. In literature, a canonical version of DES was proficiently applied in [6], as well as SAS in [7]; pushing the limit further to LES was possible with some adaption, as shown in [8]. However, no studies had yet tried to apply the SBES formulation to this family of problems at the time in which this investigation took place.

In evaluating the best compromise for timestep size, different solutions have been tried.

$$C = \frac{u\Delta t}{\Delta x}$$

Computing the Courant equal to 1 value for the zone of interest, so the rotor refinement box, the resulting timestep was ~0.015 [s].

It became also clear that giving the hybrid approach of this simulations, simply computing the timestep required for having Courant equal to 1 everywhere is neither useful nor feasible for getting timely results. As an example, if building prisms on the SFS2 for wall function TBL management, for our simulation the timestep would have been ~3x10^{-6} [s]. For the same reason, adaptive schemes for automatic timestep computation are not suited for these applications, and the analyst should proceed beforehand with an appropriate dimensional analysis.

The settings reported in Table 2 are the ones that showed the best behaviour for each solver; best here is intended as stability and convergent trend over a long period of acquisition (~x10^{1} [s]). The quality of the result for each model however was once again strictly related to the ship orientation and will be discussed in the next chapter.

In conclusion, the best approach to time discretization fitting all simulations featured:

- 1000 iterations in RANS mode
- 2000 iterations at 5x10^{-4} [s] with 20 spatial sub-iterations
- 1000 iterations at 1x10^{-3} [s] with 20 spatial sub-iterations
- 1000 iterations at 1x10^{-3} [s] with 10 spatial sub-iterations
- 30000 iterations at 1x10^{-3} [s] with 10 spatial sub-iterations

Last step is referred to those iterations where the results were acquired to be analysed and compared in terms of frequency content and mean velocity profiles, other than computing the average computational cost. These progression of settings was functional to ensure stability of the solution and a proper convergent trend.

Another important note to make is that these numerical settings evaluation happened in the first part of the work, with acquisition times and post processing intended to compare to literature results, in order to assess which model was the most promising.

After this phase, a new set of simulations, intended to mimic the suggested setup for production runs, was performed from scratch to gather the data then provided for the rotor loads analysis. Those results will be presented in the next chapter.

Residuals in spatial sub-iterations exhibited the correct trend, decreasing on average of about one order of magnitude each time. However, the total sub-iterations per timestep necessary to have an overall decreasing trend in residuals among timesteps were strongly dependent on the flow topology (in our applications, this meant azimuth), and always over 5. 10 spatial iterations per timesteps attested to be the best overall value. Increasing the number above ten did not improve the overall trend versus simulated time.

Imposing CFL=1 everywhere or either letting the code compute an adaptive timestep automatically, were naturally the best performing approaches in convergence terms, with residuals on average two orders of magnitude less than the ones obtained with imposed timestep size. However, being the acquisition time of the goal methodology determined by the rotor dynamics, the simulations would have taken thousands of times the hours they take with the final timestep chosen.

4.4. Performance Analysis

The actual impact on the quantities used in engineering applications needed to be assessed, in order to verify which was the best possible compromise between accuracy and computational time.

All simulations were performed on the same hardware, in order to be able to compare only the performance advantages given by the model itself, and in a range where both mesh resolutions were still in the linear speedup range of parallel load sharing performance. All simulations were executed on a 512 cores setup, exploiting 16 cores nodes with intel Xeon processors.

The subset of data reported hereafter are referred to the four scale resolving simulations considered the most promising and constituting the core source of data for all the analysis.

Table 3: computational performance

Model	**SAS *(low res.)***	**SBES *(low res.)***	**SAS *(high res.)***	**SBES *(high res.)***
Average wall clock time per iteration [s]	0.559	0.387	3.595	2.188

These discrepancies are also deriving from the different pressure solver between the two formulations; the setups, as mentioned above, were found to be the best compromise between accuracy and stability for each model, and that makes this comparison relevant to the analyst who is asked to embark in a simulation of this kind.

5. AEROELASTIC ANALYSIS

Aeroelastic simulations are performed by means of a multibody model by means of MSC Adams™ software Main rotor model reproduces the fully nonlinear kinematics of the system along with blade flexibility and its aerodynamics through a panel distribution.

Conditions simulated in this context are transient rotor start up coupled with the wind described by CFD computed maps; a graphical example of such maps is shown in Figure 13 where Vx, Vy and Vz gain w.r.t. the free stream are depicted. These applied wind maps remain constant during the whole transient run-up of the rotor while the blades move inside this field. The model represents a mid-level coupling between the aerodynamics and the structural analysis, since the rotor motion do not release wake nor modifies the aerodynamic field around. This however is considered a satisfactory hypothesis, since the most critical conditions happen with very low pitch of the blades starting at null translational speed. In such conditions there is almost no lift generation by the rotor disk, and therefore no disk loading.

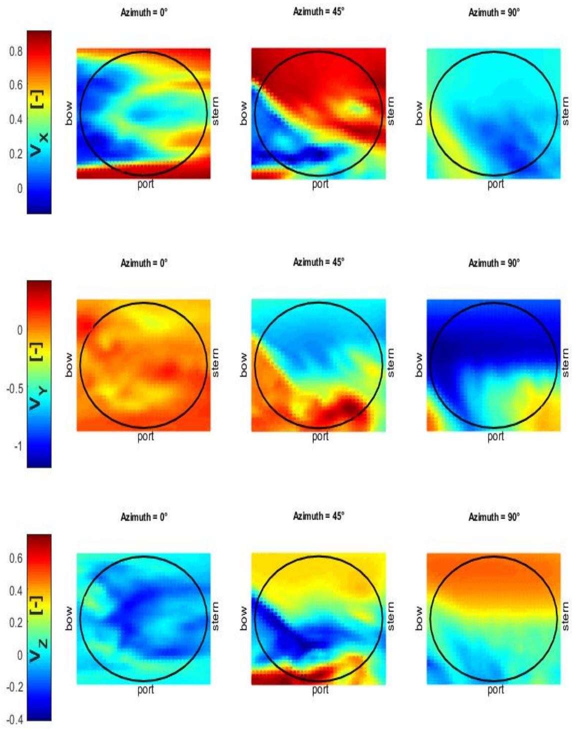

Figure 13: CFD Map example: Vx, Vy and Vz

Usually, the major focus in this kind of analyses is on the out of plane bending of the blade since the centrifugal stiffening effect is not present in the first time instants of the simulation and the blade is free to experience huge flapping motion, sometimes reaching the flap stops with consequent impact.

For these simulations, a realistic rotor model close to the ones used for the AW family, complete with all the hub controls and links, was used in order to have a reliable sensitivity to the outcomes.

6. RESULTS

The first group of simulations spaced all the possible settings in RANS and URANS simulations. RANS was set with kw-sst turbulence closure model and coupled solver for pressure-velocity fields; the solver ran for 1000 iterations, and the results were averaged over the last 100 iterations to smooth any numerical scatter that could affect such an unstable flow.

Hereafter, for the headwind condition, the simulations performed outlined a substantial difference in mean velocity distribution computation. Using the scanplane distribution defined in literature (represented in Figure 14), the four maps go from "a" to "d"

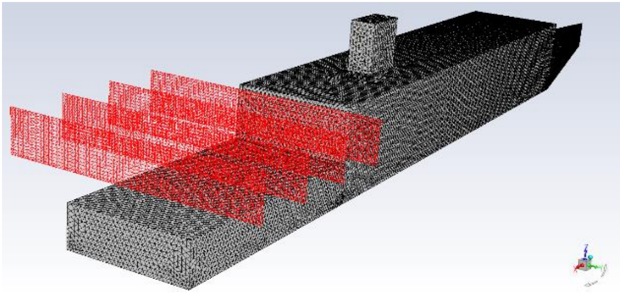

Figure 14: schematics of the scanplanes above deck

when going from aft forward. Map1c, positioned in the middle of the deck length, has been taken as reference; the main rotor mast for rotor loads simulations is in fact positioned there.

From top to bottom in Figure 15, this first comparison clearly depicts a different situation: the RANS

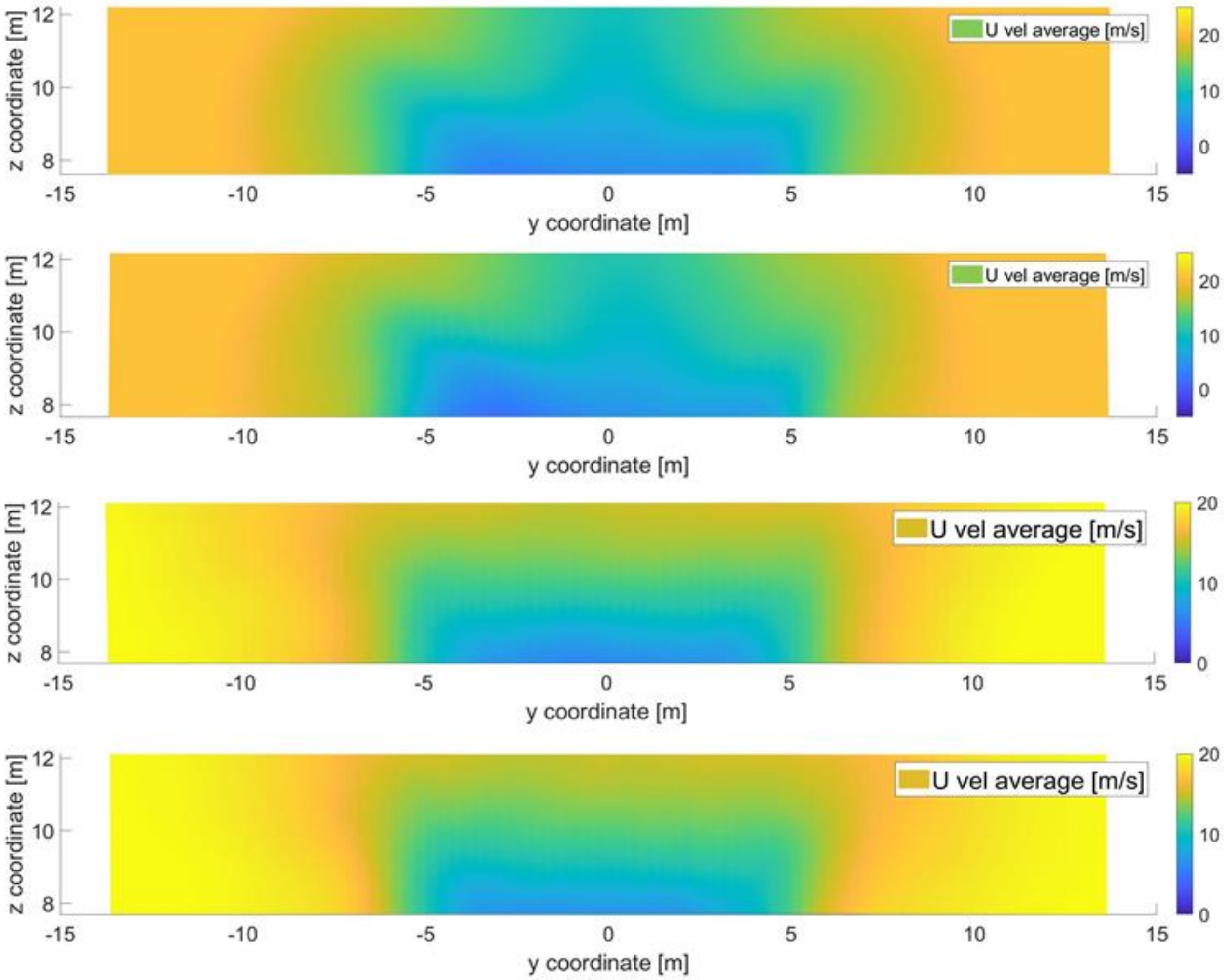

Figure 15: map1c contours comparison for average u-velocity component

modeling is inadequate in representing the turbulence structures, diffusing them excessively regardless of the mesh resolution. The central region of the deck, where is the aircraft is supposed to lie, exhibits a velocity difference sensibly higher. The contour plots are referred to the u-velocity components in order to have the immediate comprehension of the magnitude of the phenomenon, comparing them to the (around) 20 [m/s] of the freestream velocity. Scale Resolving Simulations were averaged over 30 [s].

Using the q-criterion for vorticity, the iso-surfaces in Figure 16 describe on the other hand the impact of the different mesh discretisation for a SRS: the vertical structures are sensibly different, as well as flow phenomenology. Among the tested models, as expected the URANS model do not show developed vertical structures in the same range of q as the other models.

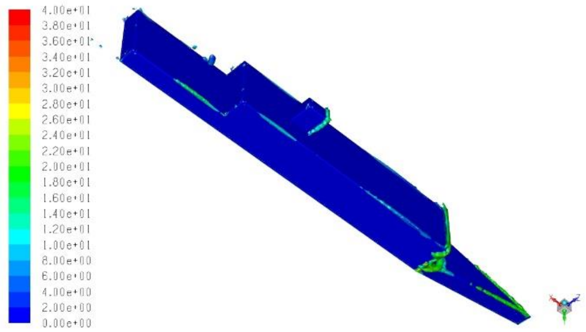

Figure 16: urans low resolution iso-q

The comparison is also relevant between the SAS and SBES modeling; the shape of the velocity difference shade impressed on map1c contours is actually different, and so are turbulent structures.

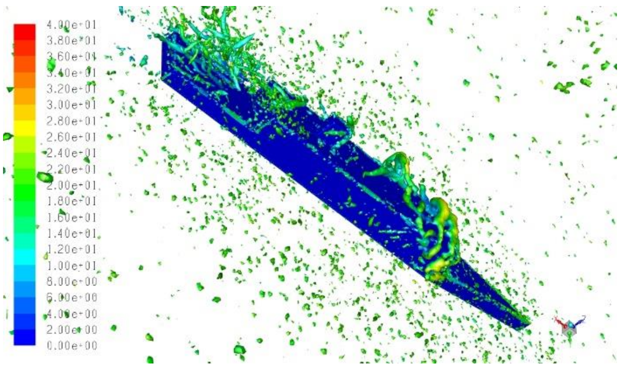

Figure 17: SAS low resolution iso-q

It is thus necessary to focus on the zone of interest; there it can be seen that even the low resolution mesh is sufficient to describe the most important vertical structures, and is also clearly depicted as the SBES model is faster in transitioning to LES mode and correctly representing turbulence right after the bluff body separation.

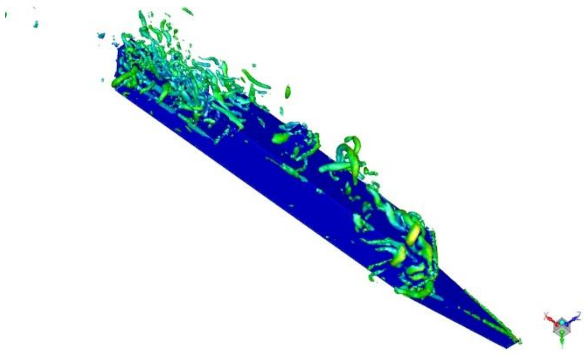

Figure 18: SBES low resolution iso-q

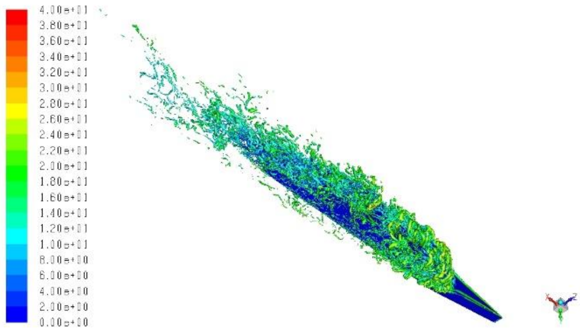

Figure 19: SBES high resolution

The PSD computation (Figure 20) happened accordingly to literature in the so called “spectra point” (reference [6]) located on map1c. It shows good agreement between the two hybrid models, even if a tendency to scatter is still present at all frequencies. The SBES model seems to adjust on a slightly higher logarithmic trend at high frequencies, but the phenomenology is overall closely similar.

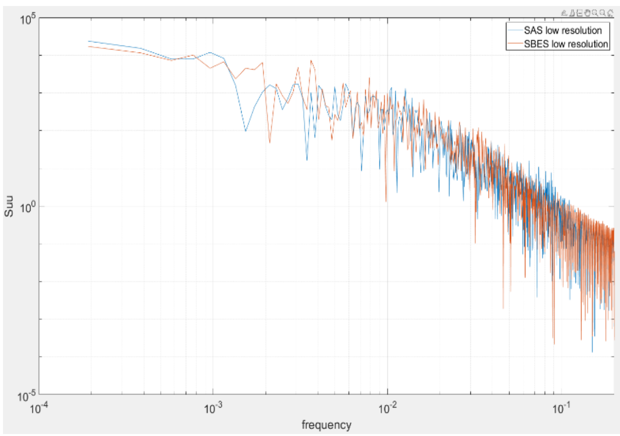

Figure 20: U velocity PSD plot at spectra point

In conclusion, the setup considered the best tradeoff features:

- A low resolution mesh was chosen, considered adequate the proper description of flow behavior in the zone of interest, as shown by the length ratio contour plots.
- A scale resolving simulation is required, giving its ability to limit excessive diffusion even on a coarser mesh, as reported by velocity profiles on scanplanes. At the same time, it is the only way to include different frequencies inside the energy content of the flow, potentially relevant in resonance analysis of the blades.
- The SBES model was chosen, giving its better performance in terms of computational time at equal accuracy and frequency content capturing ability.

Aeroelastic simulations result

This section details results associated to the aeroelastic simulations. As already mentioned, from a rotor point of view, the major focus for this type of condition is the out of plane blade bending (also referred as beam bending). For this reason, all figures here presented are associated such moment for one of the blades adimensionalized with the rotor radius.

First of all, a comparison of the complete rotor start up time history is provided for the cases with wind coming from 90 degrees and map from RANS and SBES CFD (see Figure 21). For this particular wind direction, the two approaches are comparable and also a RANS based wind map can be considered acceptable for a rotor loads estimation process.

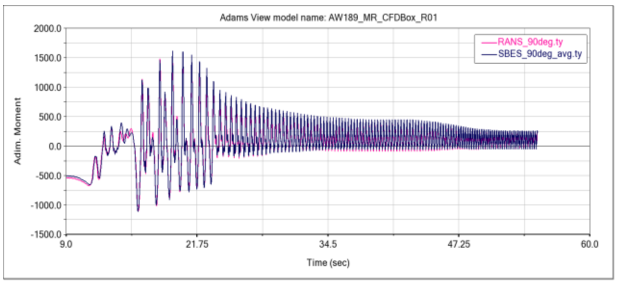

Figure 21: Blade Beam Bending, RANS vs. SBES AZ = 90°

Consider now instead the stabilized part of the simulation, when the rotor is at its nominal rotational speed, for three wind directions: 0°, 45° and 90° where the latter is simply a zoom of the previous graph (see Figure 22).

As already said for the 90° case both wind map implies similar response of rotor; considering the 45° simulations the beam bending obtained with a RANS simulation is fairly lower w.r.t. the SBES simulation especially in the peak load estimation therefore the SBES approach is leading to more severe conditions for the rotor blade. This is amplified in the 0° case where is evident that the dynamic response obtained from a RANS wind map is completely missing part of the rotor response that is instead excited by the SBES simulation.

The conclusion of this is that for some wind directions the RANS approach can be considered adequate for a rotor loads evaluation whilst for other wind direction the SBES wind map are highly recommended.

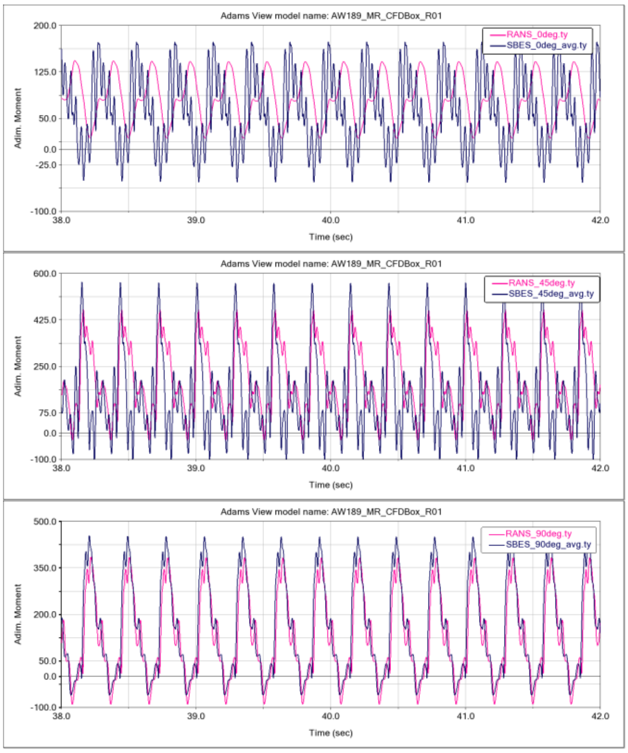

Figure 22: Blade Beam Bending, RANS vs. SBES AZ = 0°, 45° and 90° (rotor at nominal rotational speed)

The wind directions where the mean flow influence on the rotor is properly captured via RANS, are those where the rotor is not directly inside the separated wake, downstream of the ship superstructures. Moving increasingly further in azimuth from the headwind condition, the rotor box zone is less and less included inside the separation, therefore making the impact of a SRS less and less relevant on the mean value, once again confirming the highly case dependent scenario faced in this set of simulations.

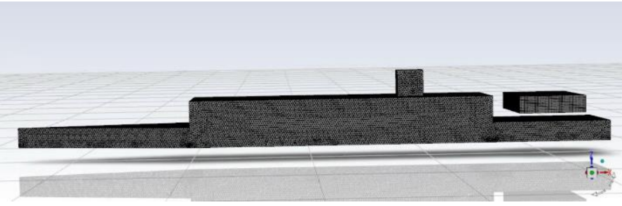

Figure 23: rotor box position on deck

Finally, for the 90° SBES case also the simulations accounting for +/- 2 sigma in the wind map evaluation are added, to consider the scenarios close to the extreme possible ones in the normal distribution expected from turbulence behavior. These two additional simulations are performed with the aim of accounting for the aerodynamic unsteadiness that is missing with the application of a time-fixed wind map. This condition was chosen given its close correlation between the average values of the tested models, therefore trying to assess the impact of unsteadiness with respect to a situation already properly captured with the legacy approach.

Anyhow, looking at Figure 24 it seems that considering this approach to account for the aerodynamic unsteadiness lead to a huge conservativism in load estimation especially for the minus two sigma wind map. Therefore, this approach might be considered inadequate in the purpose of moving towards more realistic load estimation. This criterion is also strongly case dependent, once again, and that can be seen by the fact that the plus map is the least demanding for rotor loads. Considering the case at 90°, the mean velocity effect is consistent with the recirculation bubble detached from the deck side. It is indeed the positive velocity contribution given by the 2 sigma addition that almost cancels out the negative velocity experienced by the rotor, leading to a less demanding condition.

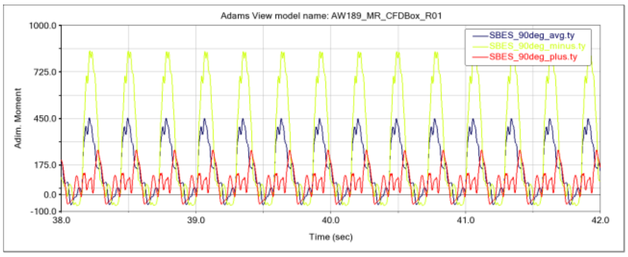

Figure 24: Blade Beam Bending, RANS at AZ = 90° (rotor at nominal rotational speed) comparison with +/- 2sigma wind map

7. CONCLUSIONS

The simulation methodology for rotor loads estimation in ship airwakes has been investigated in this paper. The outcomes outlines the following best practices:

1. A scale resolving simulation is the best choice for aerodynamics, giving the complex flow patterns present in the wake. Among others, the SBES model provides an efficient tradeoff for accuracy and cost, ensuring a fast transition to LES mode in the separated area.
2. The loads experienced by rotor blades are sensibly different when the rotor is invested by the turbulent wake and said wake is properly modeled. The transient behavior in the bending moment, the peak values and the overall simulation outputs more reliable results and different frequency contents.
3. The utterly dependent behavior of these applications on azimuth and ship geometry discourage the use of simple models for taking into account the aerodynamics of the wake in industrial applications. The reliability of the setup must be tested and verified for all conditions before concluding the best methodology.

Future Works

The conclusions reached on this paper are promising and could hardly be left at that. The confirmation on the need to simulate appropriately the airwakes for specific azimuths will further proceed trying different methods for introducing real unsteadiness inside the wind box maps.

This approach would be ideally applicable to all azimuths; the risk to consider a time-variant component of top of RANS average results is to have different levels of accuracy depending on the flow angle encountered by the ship and the rotor.

An educated approach of this kind is the mixed approach proposed in [13], even if not deemed directly applicable in industrial applications. Having to taking the data from [14] and [15], such approach clearly depicts the need for an experimental study, which is not always the best option when the number of ships and rotorcrafts to be paired starts to increase, as well as the number of possible wind speeds and azimuthal angles do for a production aircraft.

Inside Adams™ the possibility to include the unsteadiness could proceed by acquiring the time history at the hub center and superposing it on top of the wind boxes. A better approach would obviously be to provide instantaneous wind boxes and perform the aeroelastic simulation inside the actual wind speed time history. However, being the scope of this entire work to find a feasible approach that can fit inside the production time schedule, the accuracy-efficiency tradeoff of these solutions will undergo a careful evaluation. A specific dedicated interface could be defined, following the inspiring work of paper [16], where the application could vary maintaining a similar workflow.

Considering the possibility given by a radical change of paradigm, the speedup shown for these applications by studies such as [17] are surely worth taken into account, keeping an eye on the necessary resolution of resolved turbulence. As long as the required frequencies are modeled inside the aeroelastic solver, the source of aerodynamic data could change.

From the aerodynamics point of view, transforming the inner cylinder into a spherical cover could help include the hull motions inside the simulations, once again burdening even more the computational time requirement.

A possibility opened by the modular morphology given to the mesh building process is the possibility to include the atmospheric boundary layer on the sea surface activating a no slip condition on the inner portion of the inner cylinder base. As depicted in Figure 25, being the inner cylinder base the pink circle, turning on the no slip condition only on this portion will leave unaltered all the outer topology behavioural needs for meshing and flow solving. Therefore, this would allow the ship hull to encounter a more realistic incoming flow and developing a wake closer to the one experienced by the real ship. The question is that the present discretization is able or not to develop a coherent boundary layer on that surface as it was already discretized. Should the wake of the ship be impacted by this introduction with an effect deemed beneficial if compared to the results without ABL, this could be a further step of enhancement, even if marginal, as expected by the results of [11]. The contribution of this feature should affect minimally the computational time of simulations. It is also worth noticing that the impact of this feature would be intrinsically azimuth-independent, being the circular mesh equally built in any direction.

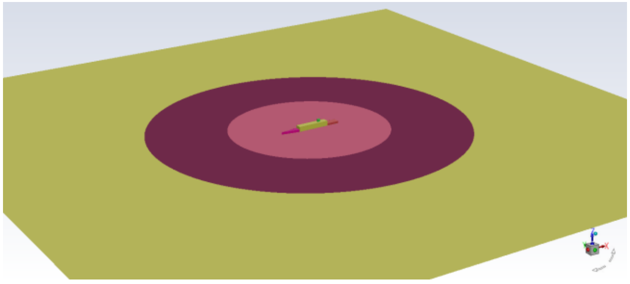

Figure 25: sea surface discretization zones

Author contact:

Gregorio Frassoldati
gregorio.frassoldati@leonardo.com
gregorio.frassoldati@uniroma3.it

Cristiano Capizzi cristiano.capizzi@leonardo.com

Davide Prederi davide.prederi@leonardo.com

Stefano Melone stefano.melone@leonardo.com

8. REFERENCES

Literature references for the present study are listed below in order of citation.

1. Yuan, W., Wall, A., and Lee, R., "Combined numerical and experimental simulations of unsteady ship airwakes," *Computers and Fluids*, Vol. 172, June 2018, pp. 29-53. DOI: 10.1016/j.compfluid.2018.06.006.
2. Popinet, S., Smith, M., and Stevens, C., "Experimental and numerical study of the turbulence characteristics of air flow around a research vessel," *Journal of Atmospheric and Oceanic Technology*, Vol. 21, (10), 2004, pp. 1574-1589.
3. Kaaria, C. H., Forrest, J. S., Owen, I., and Padfield, G. D., "Simulated aerodynamic loading of an SH-60B helicopter in a ship's airwake," 35th European Rotorcraft Forum, Hamburg, Germany, September 21-25, 2009.
4. Watson, N. A., Owen, I., and White, M. D., "Piloted Flight Simulation of Helicopter Recovery to

the Queen Elizabeth Class Aircraft Carrier," *Journal of Aircraft*, Vol. 57, (4), Jul.-Aug. 2020, pp. 742-760. DOI: 10.2514/1.C035733.

5. Sharma, A., Padthe, A., and Friedmann, P. P., "Helicopter Shipboard Landing Simulation Including Wind, Deck Motion and Dynamic Ground Effect," *Journal of Aircraft*, Vol. 58, (3), May-June 2021, pp. 467-486. DOI: 10.2514/1.C035973.

6. Forrest, J. S., and Owen, I., "An investigation of ship airwakes using Detached-Eddy Simulation," *Computers and Fluids*, Vol. 39, November 2009, pp. 656-673. DOI: 10.1016/j.compfluid.2009.11.002.

7. Shukla, S., Singh, S. N., Sinha, S. S., and Vijayakumar, R., "An Investigation of Ship Airwakes by Scale Adaptive Simulation," *the International Journal on Marine Navigation and Safety of Sea Transportation*, Vol. 14, (2), June 2020, pp. 471-475. DOI: 10.12716/1001.14.02.27.

8. Thornber, B., Starr, M., and Drikakis, D., "Implicit Large Eddy Simulation of Ship Airwakes," *Aeronautical Journal*, Vol. 114, (112), 2010, pp. 715-736.

9. Hodge, S. J., Zan, S. J., Roper, D. M., Padfield, G. D., and Owen, I., "Time-Accurate Ship Airwake and Unsteady Aerodynamic Loads Modeling for Maritime Helicopter Simulation," *Journal of the American Helicopter Society*, Vol. 54, April 2009, pp.1-16. DOI: 10.4050/JAHS.54.022005.

10. Crozon, C., Steijl, R., and Barakos, G. N., "Numerical Study of Helicopter Rotors in a Ship Airwake," *Journal of Aircraft*, Vol. 51, (6), Nov.-Dec. 2014, pp. 1813-1832. DOI: 10.2514/1.C032535

11. Seth, D., Leishman, J. G., Gnanamanickam, E., and Zhang, Z., "Time-Resolved Ship Airwake Measurements in a Simulated Atmospheric Boundary Layer," *Journal of Aircraft*, Vol. 58, (3), May-June 2021, pp. 624–649. DOI: 10.2514/1.C035886.

12. Forrest, J. S., Hodge, S. J., Owen, I., and Padfield, G. D., "An investigation of ship airwake phenomena using time-accurate CFD and piloted helicopter flight simulation," 34th European Rotorcraft Forum, Liverpool, UK, September 16-19, 2008.

13. Taymourtash, N., Zanotti, A., Gibertini, G., and Quaranta, G., "Stochastic Simulation of Ship Airwake in Helicopter Shipboard Operation," 48th European Rotorcraft Forum, Winterthur, Switzerland, September 6-8, 2022.

14. Taymourtash, N., Zagaglia, D., Zanotti, A., Muscarello, V., Gibertini, G., and Quaranta, G., "Experimental study of a helicopter model in shipboard operations," *Aerospace Science and Technology*, Vol. 115, May 2021, pp. 1-18. DOI: 10.1016/j.ast.2021.106774.

15. Taymourtash, N., Zanotti, A., Gibertini, G., and Quaranta, G., "Simulation and Testing of Helicopter Ship Aerodynamic Interaction," 47th European Rotorcraft Forum, Glasgow, Scotland, September 7-9, 2021.

16. Moushegian, A. M., and Smith, M. J., "Aerodynamic Predictions of the Ship-Helicopter Dynamic Interface with a Dual-Solver Hybrid CFD Methodology," 48th European Rotorcraft Forum, Winterthur, Switzerland, September 6-8, 2022.

17. Urban, E., Ashok, S., and Rauleder, J., "Computationally Efficient Ship Airwake Simulations for Rotorcraft Shipboard Operations Using a GPU-Accelerated Lattice-Boltzmann Solver," 48th European Rotorcraft Forum, Winterthur, Switzerland, September 6-8, 2022.